JOURNAL OF THE STRUCTURAL DIVISION

ROUGH CRACKS IN REINFORCED CONCRETE[a]

By Zdeněk P. Bažant,[1] F. ASCE and Pietro Gambarova,[2] M. ASCE

NATURE OF PROBLEM

Due to the aggregate interlock on their surfaces, cracks in reinforced concrete transmit substantial shear forces. This fact has been known for a long time, but in limit design it has usually been disregarded arguing that the friction is highly variable and should be neglected (in order to be on the safe side). This argument is, however, false (7). The reason is the dilatancy of the crack. A shear slip of crack surfaces cannot occur at constant crack opening displacement if the normal stress across the crack surface is constant. Rather, the slip is always accompanied by an increase of the crack opening (relative normal displacement, width), and if the opening is restrained then a large compressive stress is induced on the crack surface. The compressive stress must be balanced by tensile forces in the reinforcement, which are in addition to those needed to balance the applied tensile forces. Consequently, taking crack friction into account generally leads to a heavier rather than a lighter reinforcement, and thus a neglect of friction is seen to be generally on the unsafe side (7).

In finite element analysis, shear transfer across the cracks was introduced by Suidan and Schnobrich (29) reducing the shear modulus G by a shear transfer factor α_s ($0 \le \alpha_s \le 1$). However, the frictional shear stress cannot exist without a normal compressive stress across the crack, and development of a compressive stress due to crack slip has not been considered. The significance of this effect was brought to light by recent experimental results, which also revealed that the phenomenon of shear transfer is highly nonlinear. The experimental data presently available (8,9–12,14–15,27,28,30–32), although far from complete, make it possible to develop a much more realistic model. We choose it as the objective of this work.

Note.—Discussion open until September 1, 1980. To extend the closing date one month, a written request must be filed with the Manager of Technical and Professional Publications, ASCE. This paper is part of the copyrighted Journal of the Structural Division, Proceedings of the American Society of Civil Engineers, Vol. 106, No. ST4, April, 1980. Manuscript was submitted for review for possible publication on February 26, 1979.

[a]Presented at the April 2–6, 1979, ASCE Convention and Exposition and Continuing Education Program, held at Boston, Mass. (Preprint No. 3579).

[1]Prof. of Civ. Engrg., Northwestern Univ., Evanston, Ill.

[2]Postdoctoral Research Assoc., Northwestern Univ., Evanston, Ill.; Assoc. Prof. on leave from Politecnico di Milano, Italy.

We will consider in-plane forces in a concrete wall (slab, plate, shell) reinforced by a regular net of steel bars. Our attention will be limited to monotonic loading (i.e., unloading and cyclic loading are excluded) and will be directed primarily to situations in which the failure occurs by tensile yielding of the bars rather than compression or shear of concrete. This is usually the case if at least one principal internal force is tensile and not small compared to the other ones. We will adhere to the following customary assumptions: (1) The reinforcing bars are sufficiently densely distributed and can be considered "smeared"; (2) the cracks are parallel and sufficiently densely distributed; and (3) the reinforcing bars carry only axial forces—dowel action across the cracks and bar kinking

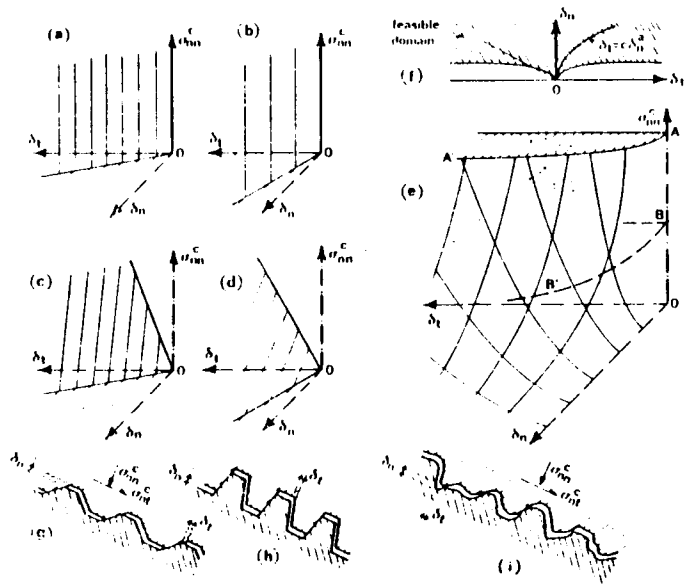

FIG. 1.—Stress-Displacement Surfaces (a)-(f) and Crack Morphology (g)-(i)

is neglected. Both of these effects can actually be quite significant, but sufficient test data are lacking.

The principal results of this work were outlined and analyzed at a recent conference (4) in the context of nuclear containments.

Theory of Stress-Displacement Relations for Rough Cracks.—Consider a single crack that is planar but microscopically rough (Fig. 1). Let δ_n and δ_t represent the relative normal and tangential displacements of crack surfaces ($\delta_n \ge 0$); let δ_n = crack opening (width); and let δ_t = crack slip. The associated forces which give a proper work expression are the normal stress σ^c_{nn} ($\sigma^c_{nn} < 0$ negative for compression) and the shear stress σ^c_{nt} where subscripts n and t refer to the normal and tangential directions, and the suffix c refers to concrete.

As an average over large crack areas and many cracks, the relation between σ^c_{nn}, σ^c_{nt} and δ_n, δ_t may be considered to be a material property, similar to stress-strain relations, and may be generally assumed in the form

$$\begin{Bmatrix} d\sigma^c_{nn} \\ d\sigma^c_{nt} \end{Bmatrix} = \begin{bmatrix} B_{nn} & B_{nt} \\ B_{tn} & B_{tt} \end{bmatrix} \begin{Bmatrix} d\delta_n \\ d\delta_t \end{Bmatrix} \quad \ldots\ldots\ldots\ldots\ldots\ldots\ldots\ldots (1)$$

in which B_{nn}, B_{nt}, ... are crack stiffness coefficients which depend on δ_n, δ_t, σ^c_{nn}, σ^c_{nt} and possibly also other state parameters. The matrix of B_{nn}, ..., B_{tt} may be called the crack stiffness matrix. The stress-displacement relations in Eq. 1 are analogous to the stress-strain relations of incremental plasticity.

Due to the scarcity of test data we must content ourselves, however, with a simpler and less general formulation:

$$\sigma^c_{nn} = f_n(\delta_n, \delta_t); \quad \sigma^c_{nt} = f_t(\delta_n, \delta_t) \quad \ldots\ldots\ldots\ldots\ldots\ldots\ldots\ldots (2)$$

which is analogous to the deformation theory (total strain theory) of plasticity and inevitably has the same weakness—namely that Eq. 2 gives a response that is independent of the loading path in the (δ_n, δ_t) plane, whereas Eq. 1 would in general give a path-dependent response, which must normally be expected of inelastic behavior. Differentiating Eq. 2 and comparing the result to Eq. 1 we conclude that

$$B_{nn} = \frac{\partial f_n}{\partial \delta_n}, \quad B_{nt} = \frac{\partial f_n}{\partial \delta_t}, \quad B_{tn} = \frac{\partial f_t}{\partial \delta_n}, \quad B_{tt} = \frac{\partial f_t}{\partial \delta_t} \quad \ldots\ldots\ldots\ldots\ldots\ldots\ldots\ldots (3)$$

This means that, as a consequence of assuming Eq. 2, our stiffness coefficients satisfy the integrability conditions

$$\frac{\partial B_{nn}}{\partial \delta_t} = \frac{\partial B_{nt}}{\partial \delta_n}, \quad \frac{\partial B_{tn}}{\partial \delta_t} = \frac{\partial B_{tt}}{\partial \delta_n} \quad \ldots\ldots\ldots\ldots\ldots\ldots\ldots\ldots (4)$$

Certain properties of the stress-displacement relations may be deduced by considering idealized crack surface morphologies. Most simply, one can imagine the crack surface as a regular array of trapezoidal asperities (Fig. 1). If they are rigid, the response surface of normal stress σ^c_{nn} as a function of δ_n and δ_t has the form shown in Figs. 1(*a*) and 1(*b*) and if the asperities elastically deform under the contact forces, the response surface looks as shown in Figs. 1(*c*) and 1(*d*). The response surface for a general irregular crack surface may be imagined as a certain superposition (most simply, a weighted sum) of the surfaces in Figs. 1(*c*) and 1(*d*), resulting in a surface of the type pictured in Fig. 1(*e*). We could speculate on the superposition rule on the basis of the statistics of asperity shapes and the number of contact points as a function of δ_n and δ_t. However it would be too hypothetical to engage in such arguments and we will exploit the models in Fig. 1 merely intuitively for introducing the general properties to be expected. These are:

1. The case $\delta_n < 0$ is meaningless and impossible, and always $\sigma^c_{nn} \leq 0$ (compression).

2. Since the surface asperities are irregular and deformable, they engage in contact at different displacements, and since the number of contact points may be considered infinite, the resulting stress-displacement relations may be considered to be continuous and smooth [Fig. 1(*e*)].

3. For $\delta_t = 0$ and $\delta_n > 0$ we must have $\sigma^c_{nn} = 0$ because the crack surfaces cannot be in contact.

4. For $\delta_n = 0$ there is full continuity in the material, i.e., there is no crack. Thus, the states where $\delta_n = 0$ and $\delta_t \neq 0$ cannot be obtained. Neither can one obtain states that are infinitely close to the axis $\delta_n = 0$, except when $\delta_t \to 0$, and so the domain of applicability ends at some finite distance from this axis, particularly at the line where σ^c_{nn} equals the compression strength f'_c of the concrete between the cracks [line AA′ in Fig. 1(*e*)]. Thus, σ^c_{nn} must exceed f'_c at $\delta_n \to 0$ ($\delta_t \neq 0$) and in particular it may tend to ∞.

5. For δ_t = constant > 0 (constant slip) and increasing δ_n, the number of contact points decreases and the elastic deformation of the asperities recovers. Consequently, $|\sigma^c_{nn}|$ as well as $|\sigma^c_{nt}|$ must decrease as the opening increases, i.e.

$$\frac{\partial |\sigma^c_{nn}|}{\partial \delta_n} = B_{nn} < 0; \quad \frac{\partial |\sigma^c_{nt}|}{\partial \delta_n} = B_{tn} < 0; \quad \text{for } \delta_t > 0 \quad \ldots\ldots\ldots\ldots (5)$$

Thus, the crack stiffness matrix is never positive definite, except for $\delta_t = 0$. So, the crack response causes a tendency for instability; however, the response is usually stabilized by the restraint provided by the reinforcement and the boundary conditions. (Because $B_{nn} < 0$, and because B_{nt} and B_{tn} must be expected to be nonzero, the stress-displacement relations cannot be modeled by springs, not even nonlinear ones).

6. If slip magnitude $|\delta_t|$ increases at δ_n = constant > 0, the asperities gradually engage in contact and also deform elastically, and so the condition

$$\frac{\partial |\sigma^c_{nn}|}{\partial \delta_t} = B_{nt} > 0; \quad \frac{\partial |\sigma^c_{nt}|}{\partial \delta_t} = B_{tt} > 0; \quad \text{for } \delta_n > 0 \quad \ldots\ldots\ldots\ldots (6)$$

should hold unless $|\delta_t|$ is so large that the asperities break.

7. From properties 3-6 it follows that the response surface of σ^c_{nn} as a function of δ_n and δ_t must exhibit a discontinuity and a singularity at the origin $\delta_n = \delta_t = 0$. This is something that would not be expected by analogy with stress-strain relations.

8. The existence of singularity calls for imposing an energy restriction. The work consumed or released by the crack as the displacements increase from zero to δ_n and δ_t must be bounded, i.e.

$$-\infty < W = \int_0^{\delta_n} \sigma^c_{nn} d\delta_n + \int_0^{\delta_t} \sigma^c_{nt} d\delta_t < \infty \quad \ldots\ldots\ldots\ldots\ldots\ldots (7)$$

The sign of the frictional stress σ^c_{nt} is the same as the sign of the slip δ_t. When the sign of δ_t changes from positive to negative, σ^c_{nn} remains the same but σ^c_{nt} changes sign. Consequently, we may write:

$$B_{nn} = \frac{\partial \sigma^c_{nn}}{\partial \delta_n}; \quad B_{nt} = \pm \frac{\partial \sigma^c_{nn}}{\partial |\delta_t|}; \quad B_{tn} = \pm \frac{\partial |\sigma^c_{nt}|}{\partial \delta_n}; \quad B_{nn} = \frac{\partial |\sigma^c_{nt}|}{\partial |\delta_t|} \quad \ldots\ldots\ldots (8)$$

in which the plus and minus signs apply for positive and negative δ_t, respectively. We see that the off-diagonal coefficients switch the sign, but the diagonal ones do not.

Empirical Stress-Displacement Relations

To choose suitable mathematical expressions for the stress-displacement relations, it is helpful to observe some simple features of the test data, especially those of Paulay and Loeber (27): (1) The curves of σ^c_{nt} versus δ_t at constant δ_n rise approximately up to the points where $\delta_t/\delta_n = 1.2$, beyond which they flatten off and reach horizontal plateaus quite abruptly; (2) the maximum shear stress slightly decreases as δ_n increases and may be considered approximately independent of δ_n; and (3) the curves of σ^c_{nt} versus δ_t at constant δ_n start with a finite slope, i.e., $B_{tt} = \partial|\sigma^c_{nt}|/\partial\delta_t < \infty$ and > 0. This slope is approximately inversely proportional to δ_n and increases as δ_t grows (locking behavior).

Based on these observations as well as the preceding theory, we see that σ^c_{nt} should depend primarily upon the ratio $r = \delta_t/\delta_n$. Examination of test data (27) further suggests that σ^c_{nn} should vary approximately in proportion to σ^c_{nt}, as in friction, and in inverse proportion to δ_n. By optimizing the fits of Paulay and Loeber's data (27) the following functions have been identified:

$$\sigma^c_{nn} = -\frac{a_1}{\delta_n}(a_2|\sigma^c_{nt}|)^p; \quad \sigma^c_{nt} = \tau_u r \frac{a_3 + a_4|r|^3}{1 + a_4 r^4} \qquad (9)$$

$$\text{with} \quad r = \frac{\delta_t}{\delta_n}; \quad \tau_u = \tau_0 \frac{a_0}{a_0 + \delta_n^2};$$

$$p = 1.30\left(1 - \frac{0.231}{1 + 0.185\delta_n + 5.63\delta_n^2}\right) \qquad (10)$$

$$\text{in which} \quad \delta_n \geq 0 \quad \text{and} \quad a_0 = 0.01D_a^2; \quad a_1 = 0.000534\frac{\text{N}}{\text{mm}}; \quad a_2 = 145\frac{\text{mm}^2}{\text{N}};$$

$$a_3 = \frac{1}{\tau_0}2.45\frac{\text{N}}{\text{mm}^2}; \quad a_4 = 2.44\left(1 - \frac{1}{\tau_0}4\frac{\text{N}}{\text{mm}^2}\right); \quad \tau_0 = 0.245 f'_c \qquad (11)$$

These expressions satisfy the properties 1–7 stipulated before.

Noting that for $\delta_t >> \delta_n$ (large slip) Eq. 9 gives $\sigma^c_{nt} = \tau_u$, we see that τ_u represents the maximum shear stress (in newtons per square millimeter) which is attained as an asymptote of the curve σ^c_{nt} versus δ_t at constant δ_n, and τ_0 = limiting value of this asymptote when $\delta_n \to 0$; f'_c is the 28-day standard cylindrical compressive strength; and D_a is the maximum aggregate size (in millimeters).

The functions in Eq. 10 appear to be valid for various concretes. [This is also supported by Fenwick's finding (15) of the similarity of his measured response curves for various concretes]. Figs. 2(*a*), 2(*b*) and 3(*a*) show the comparisons of Eqs. 9–11 with the Paulay and Loeber's test results (27). These tests represent the best ones available as their scope is sufficiently large. Further comparison is made with Fenwick's tests (15)—see Fig. 3(*b*) in which the end segments of the measured curves were not fitted because the observations have been affected by secondary diagonal and flexural cracks [Fig. 3(*b*)]. Moreover, in the case $f'_c = 16$ N/mm^2 it appeared to be necessary to reduce the values of coefficients a_3 and a_4; this may be justified by the low value of strength

of this concrete, and its high water-cement ratio. Some typical response diagrams given by Eqs. 9 and 10 are exhibited in Fig. 4.

Although the test data have been fitted well using our picture of singular behavior near the origin, it must be recognized that this picture is speculative because for very small displacements, such as $\delta_n < 0.1$ mm and $\delta_t < 0.01$ mm, the available test data reveal nothing.

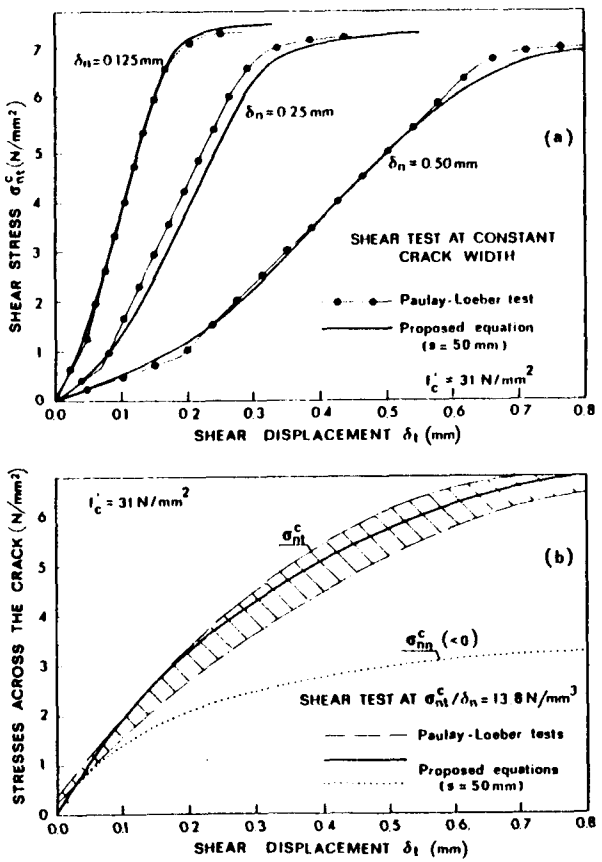

FIG. 2.—Fit of Paulay and Loeber's Test Results

The work condition in Eq. 7 restricts the admissible loading paths in the (δ_n, δ_t) plane. Every smooth and continuous path may be approximated near the origin $\delta_n = \delta_t = 0$ by the equation

$$\delta_t = c\delta_n^a \qquad (12)$$

in which c, a = constants. Substituting this, as well as Eqs. 9, 10 into Eq. 7, and carrying out the integration, one can find that the work is bounded only if $a > 1$. Furthermore, the condition that σ^c_{nn} be finite (and less than concrete strength) also admits only those paths for which $a > 1$. This indicates that

$$\frac{d\delta_t}{d\delta_n} = 0; \quad \text{for} \quad \delta_n = 0 \quad \ldots\ldots\ldots\ldots\ldots\ldots\ldots\ldots\ldots\ldots \quad (13)$$

Thus, the first displacement on the rough crack must be normal and the slip can occur only after some finite opening has already been achieved. This condition must be carefully followed in numerical calculations.

As a function of δ_n (Eq. 10), τ_u varies only mildly and may be considered to be nearly constant. Thus, Eq. 9 indicates that the shear stress σ^c_{nt} is nearly constant as long as the ratio $r = \delta_t/\delta_n$ is constant. A line of constant σ^c_{nt} in the (δ_n, δ_t) plane may be called the frictional path, and we see that such

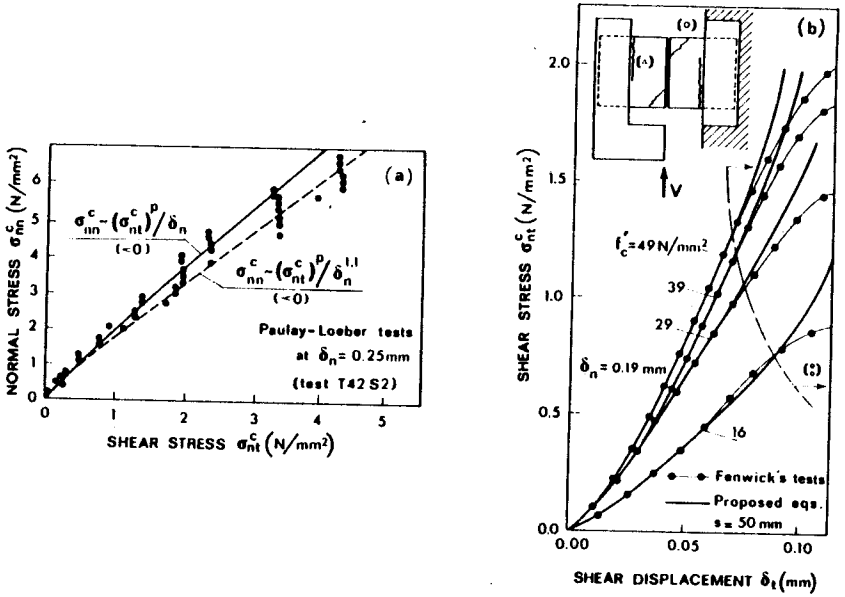

FIG. 3.—Fit of: (*a*) Paulay and Loeber's Test Results; (*b*) Fenwick's Test Results [(⊗) Failure due to Premature Formation of Flexural (Δ) and Diagonal (°) Cracks]

a path is approximately a radial line in the (δ_n, δ_t) plane—see Fig. 1(*f*). Near the origin, however, the radial line does not follow the admissible loading path (Eq. 12) and intersects the boundary of admissible states (Fig. 1(*f*). Therefore a small initial segment of the frictional path is unattainable [(dashed segment in Fig. 1(*f*)].

It is noteworthy that the maximum or asymptotic value of τ_u can be attained according to Eq. 9 for arbitrarily small δ_t, provided that $\delta_n << \delta_t$. Again, however, because of the curved boundary of the admissible domain [Fig. 1(*i*)], this is only possible at a small but finite distance from the origin.

The available tests show only a mild decline of τ_u with increasing crack opening δ_n, and they would alone be insufficient to determine the function in Eq. 10. This function results as the simplest one satisfying two reasonable conditions: (1) When δ_n exceeds the height of surface humps (which can hardly be higher than the aggregate size D_a) there can be no contact between the

crack surfaces and therefore τ_u must become vanishingly small—we choose $\tau_u = 0.01\ \tau_0$ for $\delta_n = D_a$, and solving a_0 from Eq. 10 for τ_u we get $a_0 = 0.01\ D_a^2$ (Eq. 11); (2) when $\delta_n << D_a$, the effect of δ_n upon τ_u should be negligible, or $\lim (\partial\tau_u/\partial\delta_n) = 0$ for $\delta_n \to 0$, which is satisfied by using δ_n^2 in Eq. 10 for τ_u.

For $\delta_n >> |\delta_t|$ (small slip), Eqs. 9 give

$$\sigma^c_{nn} = -A_1 \frac{|\delta_t|^p}{\delta_n^{1+p}}; \quad \sigma^c_{nt} = A_2 \frac{\delta_t}{\delta_n} \quad \ldots\ldots\ldots\ldots\ldots\ldots\ldots\ldots \quad (14a)$$

which can be easily inverted:

$$\delta_n = \frac{A_1}{(-\sigma^c_{nn})} \left|\frac{\sigma^c_{nt}}{A_2}\right|^p; \quad \delta_t = A_1 A_2^{-p-1} \frac{\sigma^c_{nt}}{(-\sigma^c_{nn})} |\sigma^c_{nt}|^p \quad \ldots\ldots\ldots\ldots \quad (14b)$$

Here $A_1 = a_1(a_2 a_3 \tau_u)^p$; and $A_2 = a_3\tau_u$. Note that a linear relation between σ^c_{nt} and δ_t/δ_n holds at the beginning of the shear test at constant δ_n, and

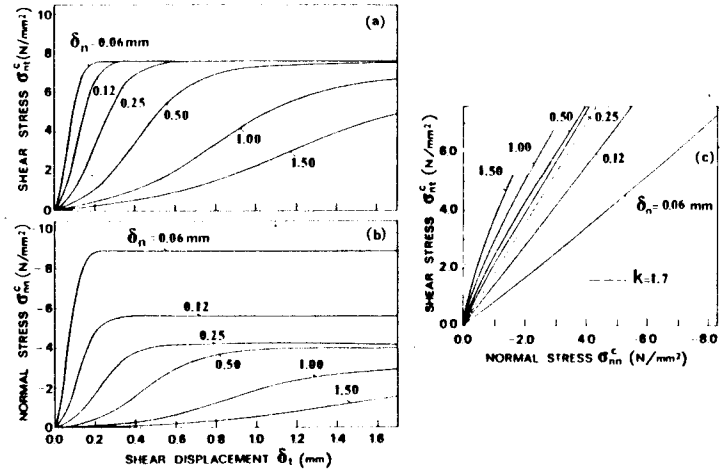

FIG. 4.—Typical Response Diagrams for Concrete with Cracks (Concrete Strength f'_c = 31 N/mm²; Crack Spacing s = 50 mm)

Fig. 4 confirms it. The secant friction coefficient is $k = -|\sigma^c_{nt}|/\sigma^c_{nn} = A_3|\delta_t|^{1-p}\delta_n^p$ in which $A_3 = A_2/A_1$. Thus $k \approx 0$ for $\delta_n >> |\delta_t|$. Substituting for a_3 and τ_u from Eqs. 10 and 11, we further have $\sigma^c_{nt} = 2.45(\delta_t/\delta_n)a_0/(a_0 + \delta_n^2) \approx 2.45(\delta_t/\delta_n)$ (in newtons per square millimeter) for small δ_n, which means that the initial slope [Fig. 2(*a*)] is independent of concrete strength; experiments tend to confirm that (15,17,30).

For $|\delta_t| >> \delta_n$ (large slip), Eq. 9 gives

$$\sigma^c_{nn} = -\frac{A_0}{\delta_n}, \quad |\sigma^c_{nt}| = \tau_u \quad \ldots\ldots\ldots\ldots\ldots\ldots\ldots\ldots\ldots\ldots \quad (15)$$

in which $A_0 = a_1(a_2\tau_u)^p$. Thus, at large slip the normal stress is inversely proportional to the crack opening, but this is only valid if δ_n is [illegible] so small

as to be out of the admissible domain [Fig. 1(*f*)]. The secant friction coefficient is $k = A_0^{-1}\tau_u\delta_n = -\tau_u/\sigma^c_{nn}$.

Recalling that the ratio of normal and tangential inelastic strains at constant normal stress is in plasticity called the dilatancy ratio, we may call $\alpha_d = |\delta_n/\delta_t|$ at constant σ^c_{nn} the crack dilatancy ratio. For $|\delta_t| << \delta_n$ (small slip), Eqs. 9 and 10 give

$$\alpha_d = \frac{\delta_n}{|\delta_t|} = a_2 a_3 \tau_u \left|\frac{a_1}{\sigma^c_{nn}\delta_n}\right|^{1/p} = \frac{a_3\tau_u}{|\sigma^c_{nt}|} \quad \ldots\ldots\ldots\ldots\ldots\ldots \quad (16)$$

We see that for $|\delta_t| << \delta_n$ the dilatancy ratio is the largest at the beginning of the shear test and declines about in inverse proportion to δ_n (because exponent

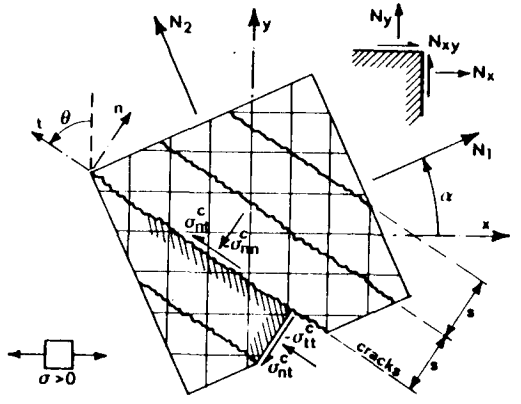

FIG. 5.—Cracked Reinforced Concrete

p is close to 1.0) as well as σ^c_{nt}. On the other hand, if $|\delta_t| >> \delta_n$, which characterizes the end of the shear test, we have

$$\alpha_d = \frac{\delta_n}{|\delta_t|} = (a_2\tau_u)^p \frac{a_1}{|\sigma^c_{nn}\delta_t|} \quad \ldots\ldots\ldots\ldots\ldots\ldots \quad (17)$$

and because σ^c_{nn} is bounded, $\alpha_d \to 0$ as $|\delta_t| \to \infty$.

Cracked Reinforced Concrete

Consider now a concrete plate (or wall, slab, shell) that is carrying only in-plane forces and is reinforced by a regular net of bars. Concrete is intersected by a system of parallel cracks of average spacing s and inclination θ with regard to the bars of x direction (Fig. 5). We will assume that the plate is sufficiently large compared to the spacing of bars and to the spacing of cracks and that the internal forces vary gradually and smoothly so that they could be assumed almost uniform over a distance of several bar and crack spacings.

By inversion of the crack stiffness matrix **B** from Eq. 1 (with stiffness coefficients given by Eq. 8), we obtain

$$\begin{Bmatrix} d\delta_n \\ d\delta_t \end{Bmatrix} = \begin{bmatrix} F_{nn} & F_{nt} \\ F_{tn} & F_{tt} \end{bmatrix} \begin{Bmatrix} d\sigma^c_{nn} \\ d\sigma^c_{nt} \end{Bmatrix} \quad \ldots\ldots\ldots\ldots\ldots\ldots \quad (18)$$

in which the square matrix represents the flexibility matrix of the crack, **F**, and $\mathbf{F} = \mathbf{B}^{-1}$.

In concrete containing many parallel cracks (Fig. 5), the deformations due to cracks may be considered continuously distributed or smeared. This treatment of cracks is commonplace in finite element analysis of concrete structures. The averaged strains due to the smeared cracks are

$$\epsilon^{cr}_{nn} = \frac{\delta_n}{s}; \quad \gamma^{cr}_{nt} = 2\epsilon^{cr}_{nt} = \frac{\delta_{nt}}{s} \quad \ldots\ldots\ldots\ldots\ldots\ldots \quad (19)$$

in which s = mean crack spacing (Fig. 5). So, according to Eq. 18,

$$\begin{Bmatrix} d\epsilon^{cr}_{nn} \\ d\epsilon^{cr}_{tt} \\ d\gamma^{cr}_{nt} \end{Bmatrix} = \begin{bmatrix} F_{nn}s^{-1} & 0 & F_{nt}s^{-1} \\ 0 & 0 & 0 \\ F_{tn}s^{-1} & 0 & F_{tt}s^{-1} \end{bmatrix} \begin{Bmatrix} d\sigma^c_{nn} \\ d\sigma^c_{tt} \\ d\sigma^c_{nt} \end{Bmatrix} \quad \ldots\ldots\ldots\ldots \quad (20)$$

or briefly $d\boldsymbol{\epsilon}^{cr} = \mathbf{D}^{cr} d\boldsymbol{\sigma}^c$ $\ldots\ldots\ldots\ldots\ldots\ldots\ldots\ldots$ (21)

Here superscript cr refers to crack. If the stiffness due to kinking of bars and their dowel action across the cracks is neglected and if the cracks are continuous, the stresses in the solid concrete between the cracks are equal to the stresses σ^c_{nn}, σ^c_{tt}, σ^c_{nt} on the crack, as already implied. Moreover, under these assumptions, the averaged strains of the reinforced concrete plate ϵ_{nn}, ϵ_{tt}, γ_{nt} (referred to as the crack directions) are the sums of the strains of the solid concrete between the cracks, ϵ^{sc}_{nn}, ϵ^{sc}_{tt}, ϵ^{sc}_{nt}, and of the strains due to the cracks, ϵ^{cr}_{nn}, ϵ^{cr}_{tt}, ϵ^{cr}_{nt}; so

$$d\boldsymbol{\epsilon} = d\boldsymbol{\epsilon}^{cr} + d\boldsymbol{\epsilon}^{sc} \quad \ldots\ldots\ldots\ldots\ldots\ldots\ldots\ldots \quad (22)$$

in which $d\boldsymbol{\epsilon} = (d\epsilon_{nn}, d\epsilon_{tt}, d\epsilon_{nt})^T$; T denotes the transpose; and $d\boldsymbol{\epsilon}^{cr}$, $d\boldsymbol{\epsilon}^{sc}$ are the analogous column matrices for strains due to the cracks and to the solid concrete between the cracks. The latter strains are related to stresses by the incremental stress-strain relations

$$d\boldsymbol{\epsilon}^{sc} = \mathbf{D}^{sc} d\boldsymbol{\sigma}^c \quad \ldots\ldots\ldots\ldots\ldots\ldots\ldots\ldots \quad (23)$$

in which $\mathbf{D}^{sc}$ is the incremental (tangential) flexibility matrix of solid concrete, which generally depends on $\boldsymbol{\sigma}^c$, $\boldsymbol{\epsilon}^c$ and possibly other state parameters. As the most realistic formulation currently available, $\mathbf{D}^{sc}$ may be considered as given by the plastic fracturing theory (5) or by linearization (1) of the endochronic theory (6). These sophisticated models are justifiable, however, only if the stresses and strains in the direction parallel to the cracks are large. In many cases, the stresses in cracked reinforced concrete are small (usually below $f'_c/3$), in which case $\mathbf{D}^{sc}$ can be considered as constant:

$$\mathbf{D}^{sc} \approx \begin{bmatrix} E^{-1} & -\nu E^{-1} & 0 \\ \text{symmetric} & E^{-1} & 0 \\ & & G^{-1} \end{bmatrix} \quad \ldots\ldots\ldots\ldots\ldots\ldots \quad (24)$$

in which E = Young's modulus; ν = Poisson ratio; and $G = 0.5\,E/(1+\nu)$ = shear modulus. Even if linear elasticity is not quite applicable, the strains often are not too large, and then one can determine the tangent flexibility matrix $\mathbf{D}^{sc}$ by differentiating some suitable total stress-strain relations for concrete, or just assume, as a simplification, incremental isotropy and evaluate the tangent shear modulus G_T and bulk modulus K_T as functions of octahedral normal and shear strains, using expressions available in the literature; in particular, those of Cedolin, et al. (13) have been employed in the computer program, and the coefficients in Eq. 24 are then determined as $G = G_T$, $E = 3(1-2\nu)K_T$, and $\nu = (E/2G) - 1$.

Substituting Eqs. 23 and 21 into Eq. 22 we obtain

$$d\boldsymbol{\epsilon} = \mathbf{D}^c d\boldsymbol{\sigma}^c; \quad \mathbf{D}^c = \mathbf{D}^{cr} + \mathbf{D}^{sc} \qquad (25)$$

in which $\mathbf{D}^c$ = incremental flexibility matrix of cracked concrete as a whole.

Now we may bring the reinforcing net into the picture. We may assume that its average strains are the same as those of the cracked concrete as a whole. This of course implies localized bond slip near the cracks because the strain of the bars is assumed not to be equal to that of solid concrete. The averaged stresses due to the reinforcing net, therefore, are

$$d\boldsymbol{\sigma}^s = \mathbf{C}^s d\boldsymbol{\epsilon} \qquad (26)$$

in which superscript s refers to steel. Since the cracks are in general inclined with respect to the reinforcing bars (Fig. 5), matrix $\mathbf{C}^s$ relative to crack coordinate axes n and t must be obtained by transformation and summing of the stiffnesses due to the bars of various directions:

$$\mathbf{C}^s = \sum_{i=1}^{N} \mathbf{R}_i^T \mathbf{C}_i^s \mathbf{R}_i, \quad \mathbf{R}_i = \begin{bmatrix} C^2, & S^2, & CS \\ S^2, & C^2, & -CS \\ -2CS, & 2CS, & C^2 - S^2 \end{bmatrix} \qquad (27)$$

$$\text{in which} \quad \mathbf{C}_i^s = \begin{bmatrix} p_i E_s(\epsilon_i), & 0, & 0 \\ 0, & 0, & 0 \\ 0, & 0, & 0 \end{bmatrix} \qquad (28)$$

Here $C = \cos\theta_i$; $S = \sin\theta_i$; θ_i = angular deviation of the crack normal from the direction of the ith bar system ($i = 1, 2, \ldots, N$); p_i = reinforcement ratio of the ith bar system. For an orthogonal net, shown in Fig. 5, we may substitute in Eqs. 27 and 28 $N = 2$, $\theta_1 = \theta$ and $\theta_2 = \theta - 90°$. The value $E_s(\epsilon)$ is the uniaxial tangent modulus of the steel bar corresponding to axial strain ϵ. Within the elastic range, E_s is constant, but in calculating large deformations beyond the service stress range it is generally necessary to consider the yielding of steel bars as well as their subsequent work-hardening. In numerical calculations described in the sequel, the yielding and work-hardening of steel bars have been considered according to the formulas of Brown and Jirsa (9) in the same manner as in Ref. 2. (However, to improve the numerical convergence in step-by-step incremental analysis, the sharp corner of the stress-strain diagram used in Ref. 2 has been eliminated by rounding it out with an exponential function that is tangent to the linear-elastic segment at 0.9 of yield strain, and tends asymptotically to the yield plateau.)

Finally, we must add the stresses due to cracked concrete and to steel bars: $d\boldsymbol{\sigma} = d\boldsymbol{\sigma}^c + d\boldsymbol{\sigma}^s$. Because, according to Eq. 25, $d\boldsymbol{\sigma}^c = \mathbf{D}^{c\,-1}\, d\boldsymbol{\epsilon}^c$, we have

$$d\boldsymbol{\sigma} = \mathbf{C}\, d\boldsymbol{\epsilon}; \quad \mathbf{C} = \mathbf{C}^s + \mathbf{D}^{c\,-1} \qquad (29)$$

in which $\mathbf{C}$ is the incremental stiffness matrix of cracked reinforced concrete, referred to crack coordinates n and t.

Eq. 29 is all that is needed for using the present theory in finite element programs. There, matrix $\mathbf{C}$ must of course be further transformed to element coordinates.

Numerical Calculations and Analysis of Results

Method of Numerical Solution.—The preceding theory allows calculating the response of cracked reinforced concrete to prescribed monotonically increasing strains or stresses. For each tensorial component, it is possible to prescribe in the loading step either the strain increment or the stress increment. Writing Eq. 29 in element form, we single out those equations for which the right-hand side values of $\Delta\sigma$ components are known, and solve the system of those equations for the corresponding $\Delta\epsilon$ components. The remaining $\Delta\epsilon$ components are the prescribed ones, and we may solve the corresponding $\Delta\sigma$ components just by evaluating the right-hand sides of the remaining equations.

A special procedure must be used during the first loading step to handle the singularity of the stress-displacement relation at $\delta_n = \delta_t = 0$. It is necessary to set $B_{nn} = 0$, assign to B_{tt} a very large value (say 10^{40}), and to B_{nt} and B_{tn} very small values (say 10^{-40}). The calculations based on these assumptions then yield $\Delta\delta_t = \Delta\gamma_{nt} = 0$ at $\delta_n > 0$ in the first loading step. When the load is exactly tangential, one gets not only $\Delta\delta_t = 0$ but also $\Delta\delta_n = 0$, in which case one must assign to $\Delta\delta_n$ for the first loading step a small nonzero value (say, 0.001 mm). The starting value for the second step must then be obtained exactly by calculating δ_t from Eq. 14*b*, using the values of σ^c_{nn}, σ^c_{nt} and δ_n previously calculated for the end of the first step. Until a larger crack opening, such as $\delta_n > 0.02$ mm is reached, and always when $|\sigma^c_{nn}|$ is too large (close to the strength value), only forward steps (corresponding to forward difference formulas) may be used, i.e., no iteration may be carried out for the crack stiffnesses to satisfy central difference incremental formulas for the step; the crack stiffnesses for these first steps must be based strictly on the end values for the previous steps and the starting value of δ_t for each subsequent step must again be solved exactly from Eq. 14*b* using the values of σ^c_{nn}, σ^c_{nt} and δ_n calculated for the end of the preceding steps.

The numerical algorithm for load increments after the crack has opened ($\delta_n > 0.02$ mm) is as follows: (1) Using the initial values of σ^c_{nn}, σ^c_{nt}, δ_n, δ_t, calculate the tangent crack stiffnesses (Eq. 8); (2) then evaluate tangent flexibilities for Eq. 26, matrix $\mathbf{D}^{cr}$ (Eq. 21), matrix $\mathbf{D}^{sc}$ (Eq. 23), total flexibility matrix $\mathbf{D}$ (Eq. 25); (3) then calculate tangent stiffness matrix of reinforcement (Eqs. 27, 28) and the total tangent stiffness $\mathbf{C}$ (Eq. 29); (4) finally, solve the load increment using Eq. 29 (this may involve finite element analysis); moreover (5) to improve accuracy, steps 1–4 may be several times iterated evaluating the crack and material properties from the average values of displacements, stresses and strains obtained in the previous calculation.

Fits of Test Data.—In fitting the available test data for reinforced concrete specimens, we must model several types of tests. Some types of tests (e.g., those of Paulay and Loeber, Fenwick, and Houde and Mirza) are made by keeping the crack width δ_n constant and equal to a prescribed value. This condition is achieved by varying the distance between the steel platens that support the two blocks of the concrete specimen [see Fig. 3(*b*)], according to the signals of several strain gages spanning across the preformed crack. In this way the effect of solid concrete deformation ϵ_{nn}^{sc} on gage signal is almost wiped out (except for that of the narrow strip spanned by the strain gages, for which no correction was made in calculations). In such tests, the prescribed quantities are $\Delta\gamma_{nt}$, $\Delta\epsilon_{nn}$ and $\Delta\sigma_{tt}^{c}$ ($\sigma_{tt}^{c} = 0$); in each step $\Delta\epsilon_{nn}$ must be set equal in magnitude and opposite in sign to the increment $\Delta\epsilon_{nn}^{sc}$ of the solid concrete

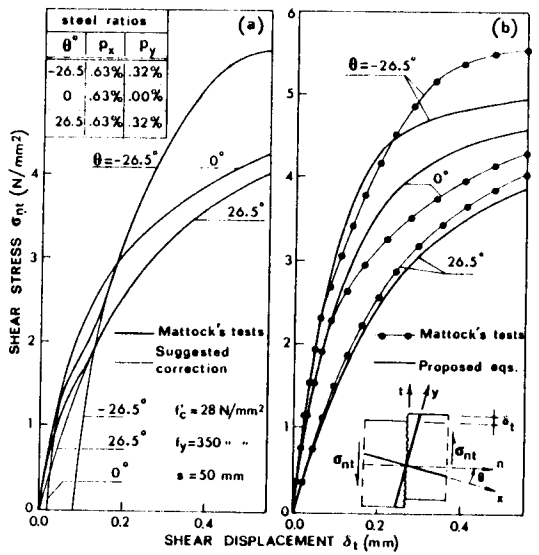

FIG. 6.—Fit of Hofbeck, Ibrahim and Mattock's Test Results for Reinforced Specimens

strain ϵ_{nn}^{sc} in the previous step, which is necessary to simulate a constant crack opening. In these tests the boundary condition $\sigma_{tt}^{c} = 0$ is however questionable because the shape of the blocks (with overlaps beyond the crack length) as well as the attachement to the steel platens does not allow free extension parallel to the crack, and so the conditions $\epsilon_{tt} = 0$ and $\sigma_{tt}^{c} = 0$ would be equally reasonable. This question is however unimportant because the numerical results obtained for $\sigma_{tt}^{c} = 0$ and $\epsilon_{tt} = 0$ are practically the same.

In another type of test (e.g., those of Mattock), two blocks are forced to slip at σ_{nn}^{c} = constant; in this case the prescribed quantities are $\Delta\gamma_{nt}$, $\Delta\sigma_{nn}^{c}$ and $\Delta\sigma_{tt}^{c}$ ($\sigma_{tt}^{c} = 0$). Tests of still another type (those of Taylor) have been performed at constant ratio $\gamma_{nt}/\epsilon_{nn}$ of overall specimen deformation, in which case $\Delta\gamma_{nt}$, $\Delta\epsilon_{nn}$ and $\Delta\sigma_{tt}^{c}$ (or $\Delta\epsilon_{tt}$) are prescribed ($\sigma_{tt}^{c} = 0$ or $\epsilon_{tt} = 0$). Achieving the desired test conditions seems to be however very difficult in these last tests, as already pointed out by Houde and Mirza (13).

The calculated fits of the results of Hofbeck, Ibrahim and Mattock's slip tests of cracked concrete specimens with steel bars at various angles are exhibited in Fig. 6. The mean crack spacing was assumed as s = 50 mm. The actually measured response diagrams have been horizontally shifted [Fig. 6(*a*)] because

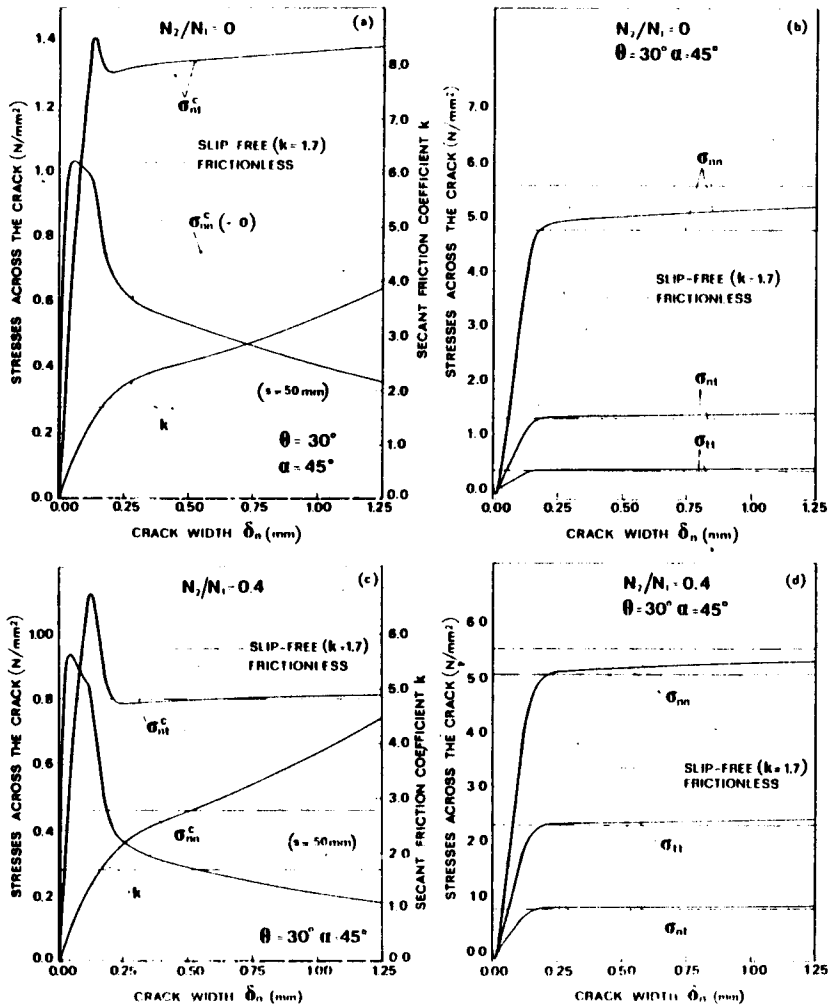

FIG. 7.—Typical Calculated Diagrams for Proportional Stressing, Compared to the Frictionless and Slip-Free Limit Loads (Concrete: f'_c = 28 N/mm²; Steel: f_y = 280 N/mm²; $p_x = p_y = 0.02$)

there was an inexplicable sudden increase of slope at the shear stress of 2 N/mm², which was probably caused by some extraneous effect. The shifts were assumed to be such that the upper part of the response curve could be smoothly extended into the origin. The agreement of the fits in Fig. 6 is not

too close for $\delta_t > 0.2$ mm, but the fact that the measured response was stiffer could be explained by dowel action of steel bars (in the cases $\pm 26.5°$) neglected in calculations.

Slip-Free Limit Design.—The response diagrams calculated in Fig. 7 allow evaluation of the previously proposed slip-free concept of limit loads of net-reinforced concrete (7). The dashed horizontal lines indicate the limit values of the applied stresses according to the classical frictionless approach, while the dash-dot lines represent the limit values for friction coefficient $k = 1.7$ according to the new slip-free design concept. The latter concept can never give higher limit load values than the frictionless approach because the steel must not only balance the applied loads but must also resist the dilatancy of the cracks and balance the normal compressive stress necessary to produce friction on the cracks.

It was previously argued (7) that the limit loads according to the new slip-free approach should correspond to the beginning of the rapid rise of deformation

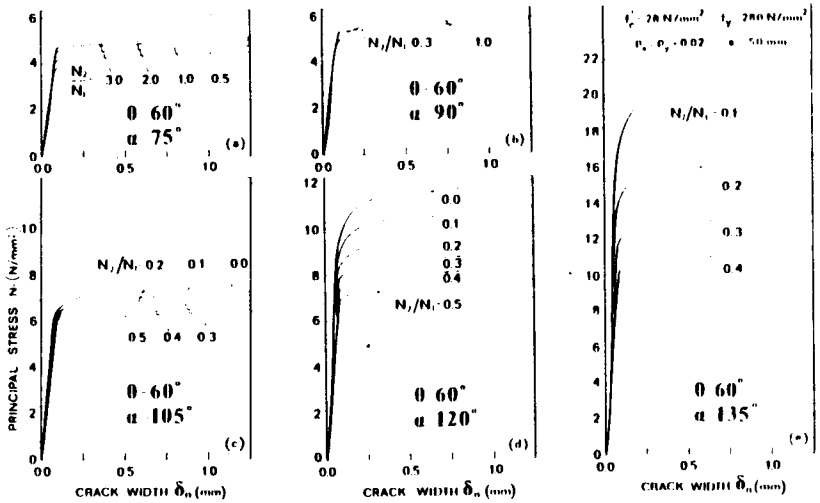

FIG. 8.—Principal Stress N_1 versus Crack Width, for Various Principal Stress Ratios and Inclinations of Principal Directions

(beginning of large crack slip), associated with the start of wide crack opening. And we see from Fig. 7 that this is indeed true.

As far as the classical frictionless concept is concerned, we notice that its limit loads are not approached even for crack opening as wide as 1.25 mm. The discrepancy between the design concepts is also seen in the normal stress plots in Fig. 7. Whereas the frictionless approach corresponds to zero normal stress, the slip-free approach gives values which correspond roughly to the correct normal stress values for the crack opening width at which a rapid increase of crack opening begins. The value $k = 1.7$ for the secant friction coefficient is generally at the low side, except for very small strains [Figs. 7(*a*) and 7(*c*)]. The maximum and the minimum points of the curves of the shear stress σ'_{nt} corresponds to the yielding of the x oriented and y or[illegible]ed bars, respectively.

Response for Various Loadings.—Fig. 8 shows calculated diagrams of the applied tensile stress N_1 as a function of crack width, for various values of the ratio $m = N_2/N_1$ and of the N_1 inclination α (Fig. 5). For each set of values (m, α) and for successive increments N_1 of the principal tensile stress N_1, the loading process is that of proportional stressing, which is characterized, according to Mohr's circle, by the conditions: $\Delta\sigma_{nt}/\Delta\sigma_{nn} = \sigma_{nt}/\sigma_{nn} = (1 - m) \sin^2(\alpha - \theta)/A$, $\Delta\sigma_{tt}/\Delta\sigma_{nn} = \sigma_{tt}/\sigma_{nn} = [(1 + m) - (1 - m) \cos 2(\alpha - \theta)]/A$ in which $A = 2\,\Delta\sigma_{nn}/\Delta N_1 = (1 + m) + (1 - m) \cos 2(\alpha - \theta)$. The results indicate that the effect of varying inclination of reinforcing bars relative to the crack is quite strong.

For design purposes, it is most safe to assume that concrete may contain

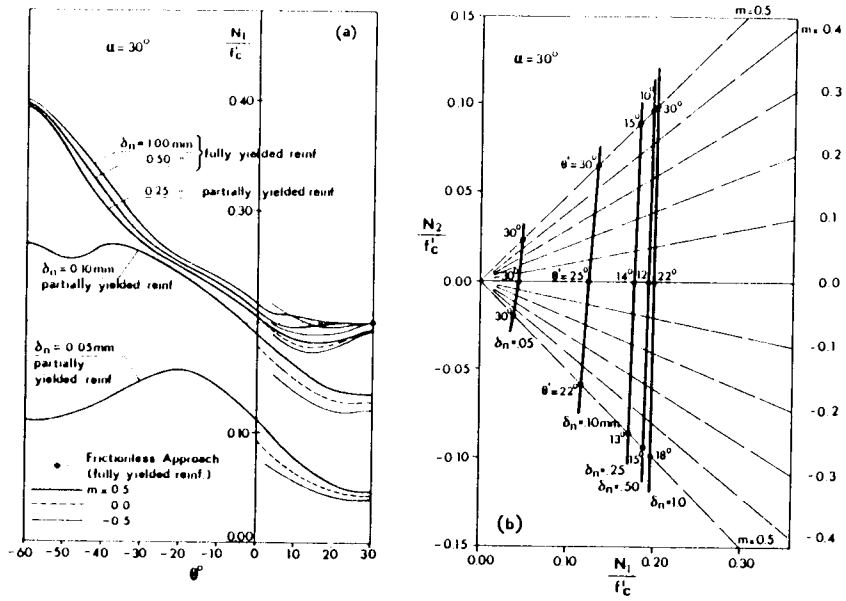

FIG. 9.—Typical Design Diagrams for Crack Width: (*a*) Principal Tensile Stress N_1 versus Crack Inclination θ for Various Crack Widths and Principal Stress Ratios; (*b*) N_2-N_1 Envelopes of Maximum Crack Width (Concrete: $f'_c = 28$ N/mm²; Steel: $f_y = 280$ N/mm²; $p_x = p_y = 0.02$; Crack Spacing $s = 50$ mm)

cracks of any direction. This is because any preload or shrinkage and temperature stresses may have caused the cracks. The crack orientation which is decisive for design is the one which gives the most unfavorable result. Running the incremental computations for various ratios $m = N_2/N_1$, and for various crack angles, θ, [Fig. 9(*a*)] it is possible to find for any given load inclination, α, the minimum value of load N_1 that produces a given crack width δ_n. The lines (envelopes) of such minimum N_1 values for various crack width are shown in Fig. 9(*b*), along with the values θ' of crack angle θ for which the minimum N_1 occurs. These lines at the same time represent the maximum crack width δ_n that can be produced by a certain load N_1. It is interesting to observe

in Figs. 9(a) and 9(b) that for small crack openings (δ = 0.05–0.10 mm) the most unfavorable crack orientation is $\theta' = \alpha$ (crack normal to N_1), while for larger values of crack opening (δ_n = 0.25–0.50 mm) θ' falls between the principal direction N_1 and the reinforcement direction x. The minimum of N_1 as a function of θ is well marked on the curves in Fig. 9(a), although it is not substantially below the value corresponding to cracks normal to N_1 (θ = 30°). For very large values of crack opening (δ_n = 1.0 mm), the most unfavorable crack orientation is roughly again normal to N_1 ($\theta' = \alpha$). In this case all reinforcement yields and the minimum N_1 now approaches the value given by the frictionless approach [dotted horizontal line in Fig. 9(a)]. This does not occur for the small values of crack width because the reinforcement then yields only partially (in Fig. 9 only the x oriented bars yield for δ_n = 0.05 mm, 0.10 mm, and 0.25 mm). Noting that the lines in Fig. 9(b) are almost vertical, we conclude that the minimum load N_1 that produces a given δ_n is not substantially affected by the ratio $m = N_2/N_1$, particularly for the large crack widths. For very large δ_n the ratio m has no effect [i.e., the lines in Fig. 9(b) are straight and exactly vertical] because in frictionless approach the most unfavorable crack orientation is normal to N_1.

The effect of crack spacing is apparent from the response diagrams in Fig. 10, and is seen to be very significant. Proportional straining (i.e., increase of strains at a fixed ratio) has been assumed. The crack spacing s is considered to be given (determination of the crack spacing itself would require analysis of stability and strain localization in concrete, and of bond slip of the bars, which is beyond the scope of this work). A smaller crack spacing implies a smaller opening width of the cracks, which gives a stiffer response. Although the crack spacing does affect the maximum normal stress [Fig. 10(b)], it has almost no effect on the maximum shear stress [Fig. 10(a)]. For fixed strains or stresses, the crack opening increases almost proportionally with the crack spacing (should the deformation of solid concrete be disregarded, we would have $\delta_n = s\epsilon_{nn}$).

Fig. 10(a) reveals a tremendous variation of the secant friction coefficient $k = -|\sigma^c_{nt}|/\sigma^c_{nn}$, but for larger shear strains, $|\gamma_{nt}| > 0.008$, the value k = 1.7 recommended by Paulay appears to be an acceptable lower bound [Figs. 10(a) and 11(c)]. The shear stress value obtained by frictionless limit analysis is always much too small [Fig. 10(c)] because it results exclusively from steel and the neglected contribution of crack friction (aggregate interlock) is substantial (usually over 50%) and remains high up to very large strains (5% in Fig. 10). The frictionless approach always gives an upper bound on the applied normal stress because the compressive stress on the crack is not subtracted [Fig. 10(d)]. The same conclusions can be drawn from the case shown in Fig. 10, e.g., where the reinforcing bars of the y direction yield in tension, and the bars of the x direction yield in compression. In this case the frictionless approach gives zero shear stiffness [$\sigma^c_{nt} = 0$, Fig. 10(f)], while the slip-free approach gives limit loads rather close to those obtained with the present "Rough Crack Model."

Fig. 11 shows some further calculated response curves for proportional straining or proportional stressing. Although at constant crack opening the secant friction coefficient is nearly constant [Fig. 4(c)], for proportional straining it is seen to exhibit a tremendous variation. For not too small crack openings, the secant

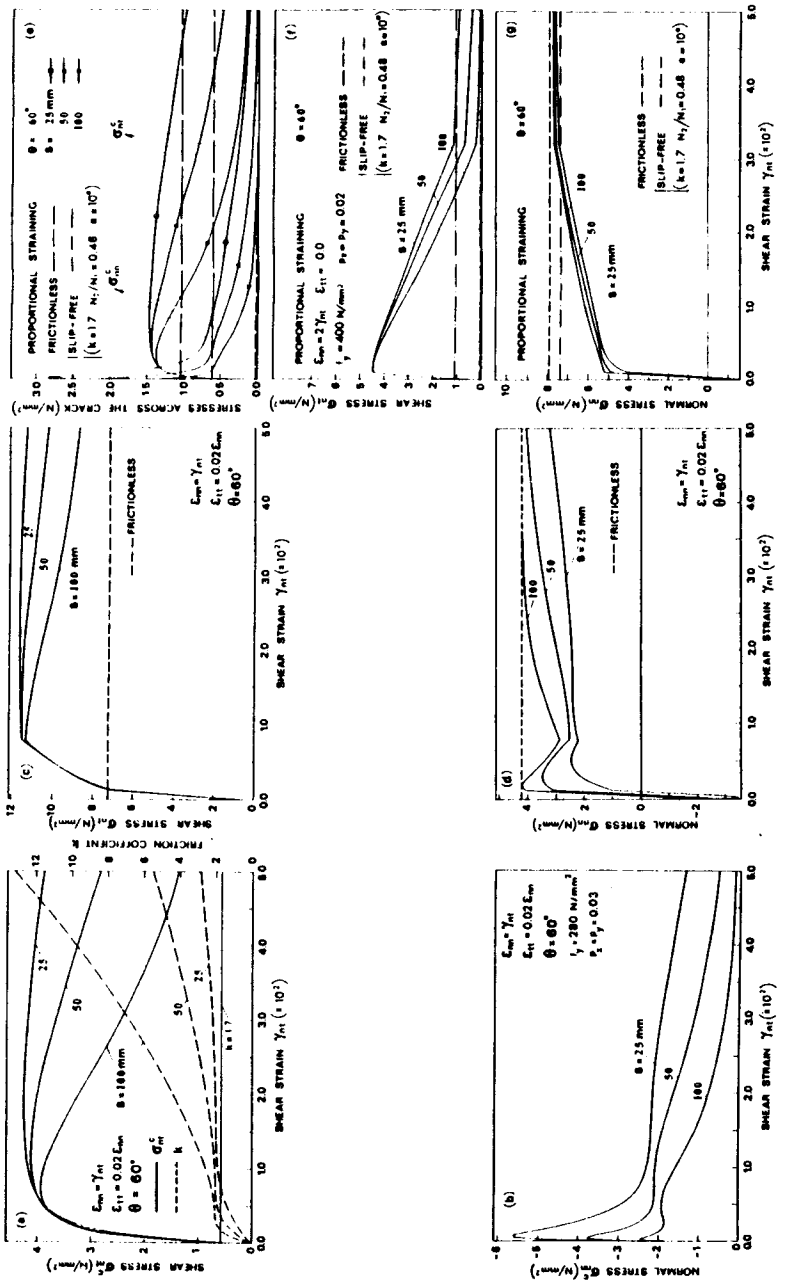

FIG. 10.—Calculated Typical Stress-Strain Diagrams for Cracked Reinforced Concrete with Various Crack Spacings Proportional Straining (f'_c = 28 N/mm²)

friction coefficient generally exceeds the value $k = 1.7$, and it is interesting to note that it can exceed this value many times. The plots of the shear stress versus the normal stress (stress paths) are nonmonotonic and exhibit reversals and; the sudden changes of slope of these curves (proportional stressing) are caused by the yield of reinforcement [Figs. 11(*d*) and 11(*e*)]. The effect of various strain ratios is seen to be very strong [Figs. 11(*b*) and 11(*c*)]. Notice in Fig. 11(*a*) also the decreasing role of crack friction (aggregate interlock) with increasing crack spacing. The great difference of response between proportional straining and proportional stressing (Fig. 11) should be also observed: In the first case the shear-to-normal stress envelopes are not affected by the yielding of the reinforcement.

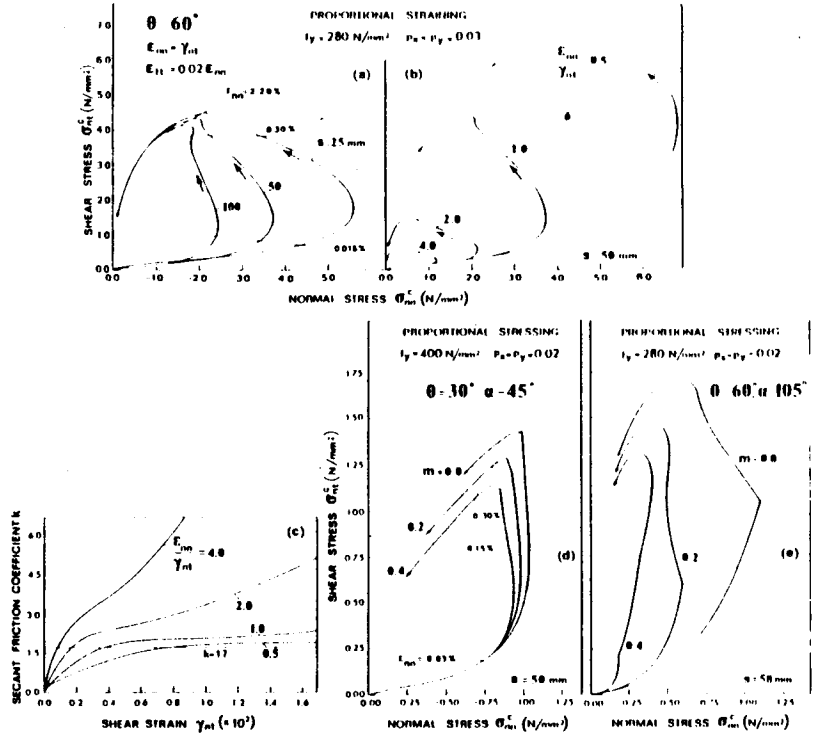

FIG. 11.—Calculated Typical Stress Paths for Cracked Reinforced Concrete: (*a*)-(*c*) Proportional Straining for Various Crack Spacings and Normal-to-Shear Strain Ratios; (*d*)-(*e*) Proportional Stressing for Various Principal Stress Ratios ($f'_c = 28$ N/mm^2)

Explicit Flexibility Matrix for Cracked Reinforced Concrete

When $\delta_n >> |\delta_t|$, substitution of Eq. 14*b* into $\epsilon_{nn} = (\sigma^c_{nn} - \nu\sigma^c_{tt})/E + \delta_n/s$ and $\gamma_{nt} = \sigma^c_{nt}/G + \delta_t/s$ allows us to get the strains as explicit algebraic functions of σ^c_{nn}, σ^c_{tt} and σ^c_{nt}, in which E, ν and G can be considered to be

variable according to the total strain (deformation)theory for the solid concrete between the cracks.

For the case $\delta_n >> |\delta_t|$ (small slip) we can also obtain an explicit expression for the incremental flexibility matrix. To this end, we differentiate Eq. 14*b* and substitute the resulting expressions for $d\delta_n$ and $d\delta_t$ into $d\epsilon_{nn} = D^c_{11}d\sigma^c_{nn} + D^c_{12}d\sigma^c_{tt} + d\delta_n/s$ and $d\gamma_{nt} = D^c_{33}d\sigma^c_{nt} + d\delta_t/s$. This yields:

$$\begin{Bmatrix} d\epsilon_{nn} \\ d\epsilon_{tt} \\ d\gamma_{nt} \end{Bmatrix} = \begin{bmatrix} D^c_{11} + A|\sigma^c_{nt}|^p\sigma^{c\,-2}_{nn}, & D^c_{12}; & \pm Ap|\sigma^c_{nt}|^p(-\sigma^c_{nn})^{-1} \\ D^c_{21}, & D^c_{22}, & 0 \\ \pm B|\sigma^c_{nt}|^{p+1}\sigma^{c\,-2}_{nn}, & 0, & D^c_{33} - B(p+1)|\sigma^c_{nt}|^p(-\sigma^c_{nn})^{-1} \end{bmatrix} \begin{Bmatrix} d\sigma^c_{nn} \\ d\sigma^c_{tt} \\ d\sigma^c_{nt} \end{Bmatrix} \quad (30)$$

in which the upper signs apply when $\sigma^c_{nt} \geq 0$ and the lower ones when $\sigma^c_{nt} \leq 0$ (like in Eq. 8); and $A = A_2^{-p}A_1/s$, $B = A_2^{-p-1}A_1/s$. If the solid concrete between the cracks behaves linearly, we have $D^c_{11} = D^c_{22} = 1/E$, $D^c_{12} = D^c_{21} = -\nu/E$ and $D^c_{33} = 1/G$. However, if there are large stresses parallel to the cracks, we may better determine D^c_{ij} using the plastic-fracturing or endochronic formulation.

For the case $|\delta_t| >> \delta_n > 0$ (large slip), the differentiation of Eq. 15 leads to the relation

$$\begin{Bmatrix} d\epsilon_{nn} \\ d\epsilon_{tt} \\ d\gamma_{nt} \end{Bmatrix} = \begin{bmatrix} D^c_{11} + A_0 s^{-1}\sigma^{c\,-2}_{nn}, & D^c_{12}, & 0 \\ D^c_{21}, & D^c_{22}, & 0 \\ 0, & 0, & F \end{bmatrix} \begin{Bmatrix} d\sigma^c_{nn} \\ d\sigma^c_{tt} \\ d\sigma^c_{nt} \end{Bmatrix} \quad (31)$$

in which $F \to \infty$.

For an approximate step-by-step loading analysis, we may utilize the matrices in Eqs. 30 and 31. The former one would apply throughout most of the (monotonic) loading process while the latter one would apply to the final collapse state at very large crack opening. The switch from the former to the latter must be made as soon as $|\sigma^c_{nt}|$ exceeds τ_u.

More accurately, we may consider for arbitrary δ_n and δ_t a continuous transition between Eqs. 30 and 31. It seems that the incremental stiffness matrix of cracked concrete (reinforcement not counted) may be approximately considered in structural analysis programs as follows:

$$\mathbf{C}^c = (1-q)\mathbf{C}_1 + q\mathbf{C}_2 \quad (32)$$

in which $q = \nu/(1+\nu)$ and $\nu = |k_m\delta_t/\delta_n|^u$, u and k_m being some positive constants (perhaps $k_m \approx 1.2$, $u \approx 3$); and $\mathbf{C}_1$ and $\mathbf{C}_2$ are the inverses of the matrices in Eqs. 30 and 31, respectively.

Note that the matrix in Eq. 31 is nonsymmetric and contains significant cross

flexibilities relating the shear and normal components. This causes that the principal directions of stresses and strains cannot remain parallel.

Further Consequences

Multi-Directional Cracking.—It is easy to generalize the preceding formulation to concrete that contains two (or more) parallel crack systems of arbitrary directions. Eq. 21 must then be written for crack systems 1 and 2 and after applying to $d\boldsymbol{\epsilon}^{cr}$ and $d\boldsymbol{\sigma}^{r}$ transformations $\mathbf{R}_1$ and $\mathbf{R}_2$ into a common coordinate system, the deformations may be added. Thus, the combined flexibility due to both crack systems is $\mathbf{D}^{cr} = \mathbf{R}_1^T\mathbf{D}_1^{cr}\mathbf{R}_1 + \mathbf{R}_2^T\mathbf{D}_2^{cr}\mathbf{R}_2$ where subscripts 1 and 2 refer to crack systems 1 and 2. The remaining calculations, Eqs. 24–29, are the same.

Bond.—It is well known that in load-carrying structures the bond between concrete and the embedded reinforcing bars is usually imperfect, damaged, and the transfer of the bond shear stress is due mainly to the interlock of surface asperities rather than adhesion. Thus, the interface resembles a crack, allowing a relative slip that is always accompanied by interface dilatancy. With increasing normal separation the normal compressive stress across the interface must decrease, and with increasing slip it must increase. Obviously the deformations due to imperfect bond, or bond cracks, may be expected to be governed by similar laws as those developed herein. Similarly as for cracks, the practice of modeling bond by spring connections between the finite elements for steel and concrete is questionable if the bond is damaged and results from interlock of asperities.

Crack Propagation Direction.—The deduced stress-displacement relations have interesting implications for the direction of crack propagation. Near the tip of a crack the opening width is small, in which case the relative displacement has been shown to be purely in the normal direction (Eq. 13). Since this condition must prevail in a sufficiently small vicinity of the crack tip, the Mode II (slip) displacement field cannot exist in case of a rough crack. Therefore, the criterion which governs the direction of propagation of a rough crack is that the Mode II stress intensity factor must vanish, i.e., $K_{II} = 0$. In other words, cracks in concrete, as well as rock, must propagate in such a direction that a pure Mode I field prevail at the crack tip. Such a propagation criterion has been considered, e.g., in the finite element analysis in Ref. 3.

Another interesting case is the crack in the interface of two dissimilar materials. The solution of the elasticity problem yields an oscillating singularity, which cannot actually take place because it implies an overlap of the crack surfaces at some points. Therefore, the crack surfaces must be in contact over some distance from the crack tip, and solutions which treat this contact as either perfectly sliding or frictional have been recently carried out. However, for materials which lead to rough cracks, it would be more realistic to rework these solutions for different contact conditions, namely those of zero slip of the opposite separated surfaces.

Rock Joints.—Continuous cracks in rock are characterized by a similar rough surface morphology and frictional contacts (joints) between the opposite surfaces. Therefore, the essentials of the present theory may be expected to also apply.

Summary and Conclusions

Derived are equations which relate the normal and shear stresses that are transmitted across a rough crack due to the contact of asperities (aggregate interlock) to the relative opening and slip displacements of the opposite crack surfaces. Average strains of concrete which contains a system of parallel continuous cracks are obtained by adding the averaged deformations due to cracks to those due to the solid concrete (possibly microcracked) between the cracks. The response of cracked concrete reinforced by a regular net of bars is then calculated using step-by-step loading. Dowel action and kinking of the bars in the cracks is neglected. Unloading and cyclic loading are not considered. The principal conclusions are:

1. Crack slip at constant opening induces normal compressive stress across the crack, and crack slip at constant normal stress causes dilatancy of the crack. An increase of crack opening reduces both normal compressive stress and the shear stress.
2. The incremental crack stiffness matrix referring to relative normal and tangential displacements is not positive definite. Because of this fact as well as the presence of off-diagonal stiffness coefficients, the stress-displacement relations cannot be modeled by springs, not even nonlinear ones.
3. The stress displacement relations for a rough crack exhibit a singularity at the initial state of zero relative displacements. The initial deformation must begin with crack opening increase at zero slip, and the numerical step-by-step algorithm must be arranged accordingly. Finite slip is impossible at zero relative normal displacements.
4. The derived stress-displacement relations satisfactorily agree with existing test data for plain concrete specimens as well as reinforced specimens.
5. The incremental stiffness matrix of cracked concrete has been derived. It is nonsymmetric and does not give parallel principal axes of stress and strain increments because a coupling of shear and normal components is present. The same must be true of the stiffness matrix of solid microcracked concrete because microcracks behave no doubt similarly as the continuous cracks.
6. Calculations of the responses of cracked net-reinforced concrete for various typical loading histories (proportional stressing or straining, shear at constant crack opening) reveal a tremendous variation of the secant friction coefficient and the dilatancy ratio for the cracks. The results are rather sensitive to the spacing of cracks.
7. The present method allows calculating the width of the cracks of known spacing as a function of the applied forces. This allows designing for a maximum crack width.
8. The previously proposed slip-free concept (with friction coefficient 1.7) yields for proportional stressing (loading) of cracked net-reinforced concrete limit loads that are found to correspond to states just before the start of a rapid increase in crack opening, while the classical frictionless approach yields limit loads that can only be achieved after very wide cracks develop.
9. Continuous cracks in concrete must propagate in such a direction that the displacement field near the crack tip be purely of Mode I (opening) type (i.e., the Mode II field cannot exist).

10. The present theory is ready for use in finite element programs that use incremental loading.

Acknowledgment

Financial support by the U.S. National Science Foundation under Grant ENG 75-14848-A01 is gratefully acknowledged. Thanks are also due to John Simon Guggenheim Memorial Foundation for supporting part of the work by awarding a Guggenheim Fellowship to the first author.

Appendix I.—References

1. Bažant, Z. P., "Endochronic Inelasticity and Incremental Plasticity," *International Journal of Solids and Structures*, Vol. 14, 1978, pp. 691–714.
2. Bažant, Z. P., and Bhat, P., "Prediction of Hysteresis of Reinforced Concrete Beams," *Journal of the Structural Division*, ASCE, Vol. 103, No. ST1, Proc. Paper 12662, Jan., 1977, pp. 153–167.
3. Bažant, Z. P., and Cedolin, L., "Blunt Crack Band Propagation in Finite Element Analysis," *Journal of the Engineering Mechanics Division*, ASCE, No. EM2, Proc. Paper 14529, Vol. 105, Apr., 1979.
4. Bažant, Z. P., and Gambarova, P., "Ductility and Failure of Net-Reinforced Concrete Shell Walls," *Transactions*, Fifth Internation Conference on Structural Mechanics in Reactor Technology, Aug., 1979 (Paper No. J4/9).
5. Bažant, Z. P., and Kim, S.-S., "Plastic-Fracturing Theory for Concrete," *Journal of the Engineering Mechanics Division*, ASCE, Vol. 105, No. EM3, Proc. Paper 14653, June, 1979, pp. 407–428.
6. Bažant, Z. P., and Shieh, C.-L., "Hysteretic-Fracturing Endochronic Theory for Concrete," *Structural Engineering Report No. 78-10/640h*, Northwestern University, Evanston, Ill., Nov., 1978.
7. Bažant, Z. P., Tsubaki, T., "Optimum Slip-free Limit Design of Concrete Reinforcing Nets," *Journal of the Structural Division*, ASCE, Vol. 105, No. ST2, Proc. Paper 14344, Feb., 1979.
8. Birkeland, P. W., and Birkeland, H. W., "Connections in Precast Concrete Construction," *Journal of the American Concrete Institute*, Vol. 63, No. 3, Mar., 1966, pp. 345–368.
9. Brown, R. H., and Jirsa, J. O., "Reinforced Concrete Beams under Load Reversals," *Journal of the American Concrete Institute*, Vol. 68, May, 1971, pp. 380–390.
10. Buyukozturk, O., "Research on Modeling Shear Transfer in Reinforced Concrete Nuclear Structures," *Report*, Department of Civil Engineering, Massachusetts Institute of Technology, Cambridge, Mass., 1979.
11. Buyukozturk, O., and Fardis, M., "Shear Transfer Model for Reinforced Concrete," *Journal of the Engineering Mechanics Division*, ASCE, Vol. 105, No. EM2, Proc. Paper 14507, Apr., 1979, pp. 255–276.
12. Buyukozturk, O., Leombruni, P., and Connor, J., "Analysis of Shear Transfer in Reinforced Concrete with Application to Containment Wall Specimens," *Research Report R72-26*, Department of Civil Engineering, Massachusetts Institute of Technology, Cambridge, Mass., June, 1979.
13. Cedolin, L., Crutzen, Y. R. J., and Dei Poli, S. D., "Triaxial Stress-Strain Relationship for Concrete," *Journal of the Engineering Mechanics Division*, ASCE, Vol. 103, No. EM3, Proc. Paper 12969, June, 1977, pp. 423–439.
14. Dulàcska, H., "Dowel Action of Reinforcement Crossing Cracks in Concrete," *Journal of the American Concrete Institute*, Vol. 69, No. 12, Dec., 1972, pp. 754–757.
15. Fenwick, R. C., "The Shear Strength of Reinforced Concrete Beams," thesis presented to the University of Canterbury, at Christchurch, New Zealand, in 1966, in partial fulfillment of the requirements for the degree of Doctor of Philosophy.
16. Hofbeck, J. A., Ibrahim, I. O., and Mattock, A. H., "Shear Transfer in Reinforced Concrete," *Journal of the American Concrete Institute*, Vol. 66, No. 13, Feb., 1969, pp. 119–128.

17. Houde, J., and Mirza, M. S., "Investigation of Shear Transfer across Cracks by Aggregate Interlock," *Research Report No. 72-06*, Department de Génie Civil, Division de Structures, École Polytechnique de Montréal, 1972.
18. Houde, J., and Mirza, M. S., "A Finite Element Analysis of Shear Strength of Reinforced Concrete Beams," *Special Publication SP42*, American Concrete Institute, 1974, pp. 103–128.
19. Jimenez-Perez, R., Gergely, P., and White, R. N., "Shear Transfer Across Cracks in Reinforced Concrete," *Report 78-4*, Department of Structural Engineering, Cornell University, Ithaca, N.Y., Aug., 1978.
20. Laible, J. P., "An Experimental Investigation in the Dynamic Analysis of Nuclear Containment Vessels," thesis presented to Cornell University, at Ithaca, N.Y., in 1973, in partial fulfillment of the requirements for the degree of Doctor of Philosophy.
21. Laible, J. P., While, R. N., and Gergely, P., "Experimental Investigation of Shear Transfer Across Cracks in Concrete Nuclear Containment Vessels," *Special Publication SP-53*, American Concrete Institute, 1977, pp. 203–226.
22. Loeber, P. J., "Shear Transfer by Aggregate Interlock," thesis presented to the University of Canterbury, at Christchurch, New Zealand, in 1970, in partial fulfillment of the requirements for the degree of Doctor of Philosophy.
23. Mast, R. F., "Auxiliary Reinforcement in Concrete Connections," *Journal of the Structural Division*, ASCE, Vol. 94, No. ST6, Proc. Paper 6002, June, 1968, pp. 1485–1509.
24. Mattock, A. H., "Shear Transfer in Concrete Having Reinforcement at an Angle to the Shear Plane," *Special Publication SP42*, American Concrete Institute, 1974, pp. 17–42.
25. Mattock, A. H., and Hawkins, N. M., "Shear Transfer in Reinforced Concrete—Recent Research," *PCI Journal*, Vol. 17, No. 2, March–April, 1972.
26. Nilson, A. H., "Nonlinear Analysis of Reinforced Concrete by the Finite Element Method," *Journal of the American Concrete Institute*, Vol. 65, No. 55, Sept., 1968, pp. 757–766.
27. Paulay, T., and Loeber, P. J., "Shear Transfer by Aggregate Interlock," *Special Publication SP42*, American Concrete Institute, 1974, pp. 1–15.
28. Paulay, T., Park, R., and Phillips, M. H., "Horizontal Construction Joints in Cast-in-Place Reinforced Concrete," *Special Publication SP42*, American Concrete Institute, 1974, pp. 599–616.
29. Suidan, M., and Schnobrich, W. C., "Finite Element Analysis of Reinforced Concrete," *Journal of the Structural Division*, ASCE, Vol. 99, No. ST10, Proc. Paper 10081, Oct., 1973, pp. 2109–2122.
30. Taylor, H. P. J., "Investigation of the Forces Carried across Cracks in Reinforced Concrete Beams in Shear by Interlock of Aggregate," *Technical Report No. 42.447*, Cement and Concrete Association, London, England, 1970.
31. Taylor, H. P. J., "The Fundamental Behaviour of Reinforced Concrete Beams in Bending and Shear," *Special Publication SP42*, American Concrete Institute, 1974, pp. 43–77.
32. White, R. N., and Holley, M. J., "Experimental Studies of Membrane Shear Transfer," *Journal of the Structural Division*, ASCE, Vol. 98, No. ST8, Proc. Paper 9145, Aug., 1972, pp. 1835–1852.

15330 ROUGH CRACKS IN REINFORCED CONCRETE

KEY WORDS: **Bonding;** Concrete; **Concrete (reinforced); Concrete structures;** Constitutive equations; **Cracking; Crack propagation;** Failure; Finite element method; **Fracture mechanics; Inelastic action; Jointed rock;** Limit analysis; Models; Numerical analysis; Plasticity; Reinforcement; **Rock mechanics;** Ultimate loads

ABSTRACT: Equations derived are which relate the normal and shear stresses transmitted across a crack due to aggregate interlock to the opening and slip displacements. Average strains due to a system of parallel continuous cracks are superimposed on the strains due to the solid concrete between the cracks. The response of cracked concrete reinforced by a regular net of bars is then calculated using an incremental loading procedure. The stress-displacement relations exhibit a singularity at the initial state of zero displacements and the initial crack opening must begin at zero slip. Responses to various types of loading are calculated and the variation of the secant friction coefficient, crack dilatancy due to slip and the effect of crack opening are studied. The theory allows designing for a maximum crack width if the crack spacing is known. The previously proposed slip-free concept yields limit loads which are found to correspond to the states just before the start of a rapid increase in crack opening, while the classical frictional approach yields limit loads that are achieved only after very wide cracks develop.

REFERENCE: Bazant, Zdenek P., and Gambarova, Pietro, "Rough Cracks in Reinforced Concrete," *Journal of the Structural Division,* ASCE, Vol. 106, No. ST4, Proc. Paper 15330, April, 1980, pp. 819-842